Dalton Transactions

PAPER

View Article Online
View Journal | View Issue

Cite this: *Dalton Trans.*, 2019, **48**, 16744

Linear-shaped Ln^{III}_4 and Ln^{III}_6 clusters constructed by a polydentate Schiff base ligand and a β-diketone co-ligand: structures, fluorescence properties, magnetic refrigeration and single-molecule magnet behavior†

Wen-Min Wang,[a,b] Li-Yuan He,[a] Xin-Xin Wang,[a] Ying Shi,[a] Zhi-Lei Wu *[b] and Jian-Zhong Cui *[b]

Received 27th August 2019,
Accepted 15th October 2019

DOI: 10.1039/c9dt03478a

rsc.li/dalton

Herein, ten new linear-shaped Ln^{III}_4 and Ln^{III}_6 clusters, with the formula $[Ln_4(acac)_6L_2(CH_3O)_2(CH_3OH)_4]\cdot xCH_3OH$ (Ln = Nd (**1**), Sm (**2**), Eu (**3**), Gd (**4**), Tb (**5**), Dy (**6**), and Tm (**8**), Hacac = acetylacetone), $[Ln_6(acac)_4L_4(CH_3O)_6]\cdot xCH_3OH$ (Er (**7**) and Yb (**9**)), and $[Lu_4(acac)_6L_2(OH)_2]\cdot 2CH_2Cl_2$ (**10**), based on a polydentate Schiff base ligand, **H_2L**, and a β-diketone co-ligand were successfully synthesized and structurally characterized. Single crystal X-ray diffraction measurements reveal that the structures of the clusters **1–6**, **8** and **10** are very similar and their central Ln(III) ions are linearly arranged Ln_4; however, the clusters **7** and **9** possess a rare linearly arranged Ln_6. The investigations on the solid-state fluorescence properties show that the clusters **2**, **3**, **5** and **6** display the characteristic lanthanum luminescence at room temperature. Magnetic studies reveal that weak antiferromagnetic interactions exist between adjacent Gd(III) ions in cluster **4**. More importantly, the cluster **4** exhibits significant MCE with the maximum $-\Delta S_m$ value of 27.96 J kg^{-1} K^{-1} at 2.0 K and 7.0 T, whereas the cluster **6** displays a slow magnetic relaxation behavior under a zero dc field with the effective energy barrier $\Delta E/k_B$ = 8.64 K and $\tau_0 = 6.98 \times 10^{-6}$ s.

Introduction

Lanthanide polynuclear clusters have been of unabated interest in single-molecule magnets (SMMs), magnetocaloric effects, luminescence materials and catalysis studies during recent years.[1–4] Among the studies of lanthanide polynuclear clusters, the investigation of Ln(III)-based clusters with single-molecule-magnet (SMM) behavior and magnetocaloric effects has attracted significant attention and great interest.[5] At the macro level, a compound usually showing a slow magnetic relaxation behavior is called a single-molecule-magnet (SMM).[6] Ever since the first double-decker mononuclear sandwich-type Ln(III)-based SMM $[Pc_2Ln]^-\cdot TBA^+$ (Ln = Tb, Dy; Pc = dianion of phthalocyanine; and $TBA^+ = N(C_4H_9)_4^+$) has been reported by Naoto Ishikawa group in 2003,[7] a large number of rare-earth SMMs have been reported in the literature.[8] With the rapid development of knowledge for coordination chemistry and magneto-chemical properties during these years, lanthanide ions, especially Dy(III) and Tb(III) ions with a large ground-state spin and a significant magnetic anisotropy, have been widely regarded as optimal candidates for the design and construction of SMMs in a number of studies in the literature.[9] In these reported studies, it appears that polynuclear Ln(III)-based clusters are more competitive and focused due to their fascinating structures and outstanding magnetic behaviors.[10] Tang and Tong's group has conducted pioneering and preeminent studies on lanthanide cluster SMMs.[11] Furthermore, as one of the hot spots of material chemistry, magnetic cooling technology is based on the magnetocaloric effect (MCE), which is highly desirable and being actively pursued due to the anticipated compactness, environmental benignness and energy efficiency.[12] Owing to their potential applications, the magnetic cooling technology may be of use in daily-life such as in fridges and air-conditioners. Magnetic refrigeration materials with large magnetocaloric effects may replace the increasingly rare and expensive helium-3 as a coolant.[13] In general, an excellent magnetic cooler should possess the features of negligible magnetic anisotropy, a large spin ground state, *S*, and high magnetic density.[14] Hence, Gd-containing

[a]*Department of Chemistry, Taiyuan Normal University, Jinzhong 030619, China*
[b]*Department of Chemistry, Tianjin University, Tianjin, 300072, China.*
E-mail: cuijianzhong@tju.edu.cn, wuzhilei03@163.com

†Electronic supplementary information (ESI) available. CCDC 1949161–1949170. For ESI and crystallographic data in CIF or other electronic format see DOI: 10.1039/c9dt03478a

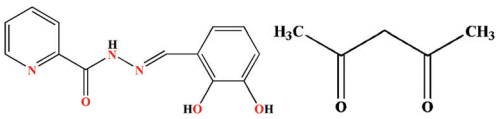

Scheme 1 The structures of H_2L (left) and Hacac (right).

compounds with small ligands are promising candidates, and a number of Gd(III)-based clusters with outstanding magnetic refrigeration properties have been reported over the past decade.[15] It should be pointed out that Zheng and Long's group has conducted good work on the magnetic refrigeration aspect of Gd(III)-based clusters.[16] These studies develop and promote the design and synthesis of lanthanide-based clusters; moreover, they also inspire the scientific researchers to explore the outstanding and excellent magnetic properties of lanthanide-based clusters.

Through the above mentioned studies, it is concluded that because of their notable and fascinating molecular topologies, polynuclear lanthanide-based clusters, especially, the Ln_4 and Ln_6 clusters, such as the [2 × 2] square grid Ln_4^{III} clusters,[17] linear shaped Ln_4^{III} clusters,[18] butterfly-shaped (or rhombus-shaped) Ln_4^{III} clusters,[19] triangle-based pyramid Ln_4^{III} clusters,[20] zigzag Ln_4^{III} clusters,[21] Y-shaped Ln_4^{III} clusters,[22] propeller-shaped Ln_6^{III} clusters,[23] and planar triangular Dy_3 + Dy_3 clusters,[24] exhibit excellent magnetic properties. Recognizing the interesting molecular structures and intriguing magnetic properties of polynuclear lanthanide(III)-based compounds, we herein report a series of approximate linear-shaped lanthanide tetranuclear and hexanuclear clusters, $[Ln_4(acac)_6L_2(CH_3O)_2(CH_3OH)_4]\cdot xCH_3OH$ (Ln = Nd (**1**), Sm (**2**), Eu (**3**), Gd (**4**), Tb (**5**), Dy (**6**), and Tm (**8**)), $[Ln_6(acac)_4L_4(CH_3O)_6]\cdot xCH_3OH$ (Er (**7**) and Yb (**9**)), and $[Lu_4(acac)_6L_2(OH)_2]\cdot 2CH_2Cl_2$ (**10**), which were constructed by the multidentate Schiff base ligand ($\mathbf{H_2L}$) and $Ln(acac)_3\cdot 2H_2O$ *via* the solvothermal method (Scheme 1). Magnetic studies reveal that cluster **4** exhibits significant MCE with the maximum $-\Delta S_m$ value of 27.96 J kg^{-1} K^{-1} (T = 2.0 K and ΔH = 7.0 T), while cluster **6** shows a slow SMM behavior under zero dc field with $\Delta E/k_B$ = 8.64 K and $\tau_0 = 6.98 \times 10^{-6}$ s.

Experimental

Materials and methods

Herein, the common solvents and chemicals used for the syntheses were of reagent grade and used without further purification. The multidentate Schiff base ligand $\mathbf{H_2L}$ was synthesized according to the previously reported method (Scheme 2).[25] The ten β-diketone salts $Ln(acac)_3\cdot 2H_2O$ (Ln = Nd, Sm, Eu, Gd, Tb, Dy, Er, Tm, Yb and Lu) were synthesized according to the method reported in the literature.[26]

Synthesis of 2-picolinyl hydrazide. A methanolic solution (10 mL) of hydrazine hydrate (5 mL) was added dropwise to a stirred solution of methyl picolinate (25 mmol) in methanol

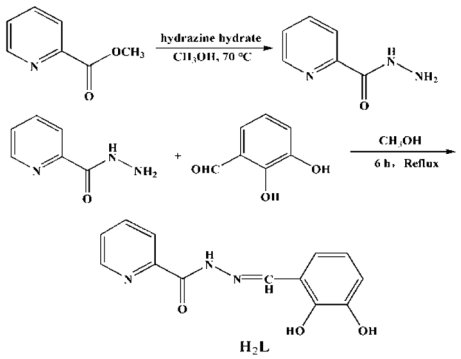

Scheme 2 Detailed outline of the synthesis of the ligand ($\mathbf{H_2L}$).

(30 mL) at room temperature. Then, the reaction mixture was heated under reflux at 70 °C for 4 h. It was then cooled to room temperature, and lots of white precipitates were obtained; the precipitates were filtered and washed with a small amount of cold methanol. The products were then dried under vacuum for 12 h. Yield = 3.05 g (89%). Anal. calcd for $C_6H_7N_3O$ (F_W = 137.14): C, 52.50; H, 5.10; N, 30.63. Found: C, 52.53; H, 5.08; N 30.67.

Synthesis of $\mathbf{H_2L}$. A mixture of 2,3-dihydroxybenzaldehyde (15.0 mmol) and 2-picolinyl hydrazide (15.0 mmol) in 50 mL of methanol was refluxed for 6 h, and lots of white precipitates were produced. Then, the precipitates were filtered and dried under vacuum for 48 h to give ligand $\mathbf{H_2L}$. Yield: 2.43 g (63%). Elemental analysis (%) calcd for $C_{13}H_{10}N_3O_3$ (F_W = 257.26): C, 60.64; H, 3.89; N, 16.33. Found: C, 60.68; H, 3.93; N, 16.29. IR (KBr, cm^{-1}, Fig. S1 in ESI†): 3298(m), 3016(w), 2946(w), 2904(w), 2834(w), 1634(s), 1584(w), 1522(w), 1471(m), 1456(m), 1420(w), 1371(w), 1333(w), 1251(s), 1204(w), 1167(w), 1120(m), 1095(w), 1077(s), 1051(w), 980(m), 950(m), 923(m), 834(m), 780(m), 731(s).

Synthesis of clusters 1–10. The procedure for the synthesis of clusters **1–10** was very similar (Scheme 3). $Ln(acac)_3\cdot 2H_2O$ (0.03 mmol) was added to a solution of $\mathbf{H_2L}$ (0.03 mmol) in 12 mL of CH_3OH/CH_2Cl_2 (v/v = 3 : 1), and then the mixture was stirred for 30 min at room temperature. Whereafter, the mixture was sealed and packed in a 20 ml glass sample vase, which was heated at 80 °C for 3 days under autogenous pressure. Then, white block crystals of **1–10** suitable for X-ray crystallography were obtained.

$[Nd_4(acac)_6L_2(CH_3O)_2(CH_3OH)_4]\cdot 2CH_3OH$ (1). Yield: 58% (based on Nd salt). Elemental analysis (%) calcd for $C_{66}H_{98}N_6O_{28}Nd_4$ (F_W = 2000.46): C, 39.59; H, 4.90; N, 4.20. Found: C, 39.63; H, 4.85; N, 4.26. IR (KBr, cm^{-1}, Fig. S1†): 3065(w), 1557(m), 1521(s), 1465(w), 1433(s), 1367(w), 1346(s), 1252(s), 1215(s), 1165(w), 1088(w), 1020(s), 912(m), 867(s), 796(w), 749(s), 686(m).

$[Sm_4(acac)_6L_2(CH_3O)_2(CH_3OH)_4]\cdot 2CH_3OH$ (2). Yield: 58% (based on Sm salt). Elemental analysis (%) calcd for $C_{64}H_{90}N_6O_{26}Sm_4$ (F_w = 1960.81): C, 39.17; H, 4.59; N, 4.28. Found: C, 39.23; H, 4.64; N, 4.21. IR (KBr, cm^{-1}, Fig. S1†): 3632(w), 3069(w), 1581(m), 1560(m), 1506(s), 1429(s), 1375(s),

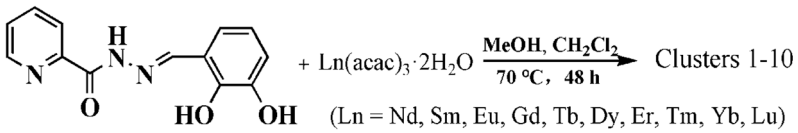

Scheme 3 Synthesis of the clusters **1–10**.

1359(s), 1249(s), 1207(s), 1177(w), 1093(w), 1051(w), 1009(s), 917(s), 862(s), 753(s), 694(s).

$[Eu_4(acac)_6L_2(CH_3O)_2(CH_3OH)_4]\cdot 2CH_3OH$ (3). Yield: 58% (based on Eu salt). Elemental analysis (%) calcd for $C_{64}H_{90}N_6O_{26}Eu_4$ (F_w = 1967.25): C, 39.04; H, 4.57; N, 4.27. Found: C, 39.10; H, 4.61; N, 4.23. IR (KBr, cm^{-1}, Fig. S1†): 3586(w), 3048(w), 2921(w), 1581(m), 1551(m), 1514(s), 1429(s), 1378(m), 1341(s), 1256(s), 1207(s), 1168(w), 1089(w), 1047(w), 1013(s), 921(s), 862(s), 786(w), 740(s), 689(m).

$[Gd_4(acac)_6L_2(CH_3O)_2(CH_3OH)_4]$ (4). Yield: 58% (based on Gd salt). Elemental analysis (%) calcd for $C_{62}H_{82}N_6O_{24}Gd_4$ (F_w = 1924.33): C, 39.91; H, 4.26; N, 4.37. Found: C, 39.88; H, 4.31; N, 4.30. IR (KBr, cm^{-1}, Fig. S1†): 2988(w), 2908(w), 1589(m), 1560(m), 1514(s), 1442(s), 1383(s), 1350(m), 1297(w), 1269(s), 1203(s), 1164(w), 1101(w), 1047(w), 1013(s), 921(s), 862(s), 828(w), 811(w), 753(s), 694(m).

$[Tb_4(acac)_6L_2(CH_3O)_2(CH_3OH)_4]\cdot CH_3OH$ (5). Yield: 58% (based on Tb salt). Elemental analysis (%) calcd for $C_{61}H_{78}N_6O_{23}Tb_4$ (F_w = 1898.97): C, 38.55; H, 4.11; N, 4.42. Found: C, 38.61; H, 4.04; N, 4.48. IR (KBr, cm^{-1}, Fig. S1†): 3384(w), 3069(w), 1594(m), 1518(s), 1475(w), 1442(s), 1383(s), 1359(m), 1265(s), 1207(m), 1176(w), 1101(w), 1051(w), 1018(s), 921(m), 857(s), 807(w), 749(s), 710(w), 694(s).

$[Dy_4(acac)_6L_2(CH_3O)_2(CH_3OH)_4]\cdot 2CH_3OH$ (6). Yield: 58% (based on Dy salt). Elemental analysis (%) calcd for $C_{64}H_{90}N_6O_{26}Dy_4$ (F_w = 2009.41): C, 38.22; H, 4.48; N, 4.18. Found: C, 38.26; H, 4.45; N, 3.23. IR (KBr, cm^{-1}, Fig. S1†): 3069(w), 1555(m), 1522(s), 1467(w), 1433(s), 1367(w), 1345(s), 1253(s), 1215(s), 1164(w), 1089(w), 1018(s), 912(m), 866(s), 795(w), 749(s), 685(m).

$[Er_6(acac)_4L_4(CH_3O)_6]$ (7). Yield: 58% (based on Er salt). Elemental analysis (%) calcd for $C_{78}H_{82}Er_6N_{12}O_{26}$ (F_w = 2607.11): C, 35.90; H, 3.15; N, 6.44. Found: C, 35.86; H, 3.19; N, 6.46. IR (KBr, cm^{-1}, Fig. S1†): 3565(w), 3077(w), 2354(w), 1606(w), 1551(s), 1518(m), 1438(s), 1387(m), 1345(m), 1301(w), 1265(s), 1203(s), 1156(w), 1097(w), 1018(s), 926(m), 853(s), 807(w), 768(s), 740(s), 685(m).

$[Tm_4(acac)_6L_2(CH_3O)_2(CH_3OH)_4]\cdot 2CH_3OH$ (8). Yield: 58% (based on Tm salt). Elemental analysis (%) calcd for $C_{64}H_{90}N_6O_{26}Tm_4$ (F_w = 2035.14): C, 37.74; H, 4.42; N, 4.13. Found: C, 37.67; H, 4.37; N, 4.09. IR (KBr, cm^{-1}, Fig. S1†): 3081(w), 2366(w), 1594(w), 1548(m), 1505(s), 1442(s), 1378(s), 1345(s), 1210(s), 1164(w), 1097(w), 1055(w), 1009(s), 926(m), 857(s), 795(w), 744(s), 689(m).

$[Yb_6(acac)_4L_4(CH_3O)_6]\cdot 2CH_3OH$ (9). Yield: 58% (based on Yb salt). Elemental analysis (%) calcd for $C_{78}H_{82}N_{12}O_{26}Yb_6$ (F_w = 2641.79): C, 35.43; H, 3.10; N, 6.36. Found: C, 35.48; H, 3.05; N, 6.41. IR (KBr, cm^{-1}, Fig. S1†): 3515(w), 3027(w), 2362(w), 1606(w), 1564(m), 1518(s), 1442(s), 1378(w), 1354(s), 1253(s), 1203(s), 1164(w), 1106(w), 1055(w), 1009(s), 933(m), 866(m), 820(w), 756(s), 740(m), 689(m).

$[Lu_4(acac)_6L_2(CH_3O)_2]\cdot 2CH_2Cl_2$ (10). Yield: 58% (based on Lu salt). Elemental analysis (%) calcd for $C_{58}H_{66}Cl_4N_6O_{20}Lu_4$ (F_w = 2008.84): C, 34.65; H, 3.29; N, 4.18. Found: C, 34.60; H, 3.35; N, 4.24. IR (KBr, cm^{-1}, Fig. S1†): 3384(w), 3069(w), 2363(w), 1581(m), 1514(s), 1451(s), 1378(s), 1354(m), 1295(w), 1265(s), 1210(s), 1168(w), 1101(w), 1051(w), 1018(s), 933(m), 871(s), 807(w), 744(s), 685(s).

X-ray crystallography

Single crystal X-ray diffraction data of clusters **1–10** were collected on a computer-controlled Rigaku Saturn CCD area detector diffractometer, equipped with confocal monochromatized Mo Kα radiation with a radiation wavelength of 0.71073 Å using the ω–φ scan technique. The structures were solved by direct methods and refined with a full-matrix least-squares technique based on F^2 using the SHELXS-2016 and SHELXL-2016 programs.[27] Anisotropic thermal parameters were assigned to all non-hydrogen atoms. Crystallographic data and structural refinement parameters are listed in Tables 1 and 2. CCDC (1949161–1949170 for clusters **1–10**)† contains the supplementary crystallographic data for this paper.

Results and discussion

Crystal structures of clusters 1–6 and 8

The single-crystal structural analyses imply that the crystals **1–6** and **8** are isostructural. Hence, the structure of cluster **6** is selected and discussed in detail (Fig. 1). Cluster **6** has a $P2_1/c$ space group in the monoclinic system with Z = 2. The centrosymmetric cluster has a nearly linear Dy_4 core with the Dy–O bond distance in the range of 2.283(5)–2.574(5) Å, and the Dy–N bond lengths are 2.475(6) and 2.622(6) Å, respectively. These bond lengths are fall in the normal range of the previously reported Dy_4 clusters.[28] The central nine-coordinated Dy1 atom is connected by eight O atoms (O1, O2, O3, O4, O5, O11, O12 and O2a) and one N atom (N1), while the central Dy2 atom is eight-coordinated with a O_7N coordination environment (Fig. S2†). The Dy1 ion possesses a distorted spherical capped square antiprism geometry, and the Dy2 ion possesses a distorted triangular dodecahedron geometrical configuration (Fig. 2), which can be confirmed by continuous-shape measurements (CShM) using SHAPE 2.0 software (Table S1†). The coordination modes of H_2L and $acac^-$ in **6** are shown as

Table 1 Crystallographic data and structure refinements for clusters **1–5**

	1	**2**	**3**	**4**	**5**
Formula	$C_{66}H_{98}N_6Nd_4O_{28}$	$C_{64}H_{90}N_6O_{26}Sm_4$	$C_{64}H_{90}Eu_4N_6O_{26}$	$C_{64}H_{90}Gd_4N_6O_{26}$	$C_{61}H_{78}N_6O_{23}Tb_4$
*M*r (g mol^{-1})	2000.46	1960.81	1967.25	1988.41	1898.97
T (K)	150.0	150.0	150.01	150.0	150.01
Cryst syst	Trigonal	Monoclinic	Monoclinic	Monoclinic	Monoclinic
Space group	$R\bar{3}$	$P2_1/c$	$P2_1/c$	$P2_1/c$	$P2_1/c$
a (Å)	47.810(3)	24.4789(12)	24.4547(10)	24.4700(14)	15.3614(16)
b (Å)	47.810(3)	15.0651(7)	15.0632(7)	15.0504(8)	12.8302(13)
c (Å)	9.5696(6)	20.8613(11)	20.8363(10)	20.7774(10)	35.007(4)
α (°)	90	90	90	90	90
β (°)	90	98.526(2)	98.3314(16)	98.373(2)	94.671(3)
γ (°)	120	90	90	90	90
V (Å^3)	18944(2)	7608.1(7)	7594.4(6)	7570.4(7)	6876.5(12)
Z	9	4	4	4	4
Cryst size (mm^3)	0.29 × 0.21 × 0.14	0.26 × 0.21 × 0.13	0.23 × 0.18 × 0.14	0.32 × 0.21 × 0.14	0.26 × 0.21 × 0.14
D_c (g cm^{-3})	1.578	1.712	1.721	1.745	1.834
μ (mm^{-1})	2.501	3.121	3.337	3.538	4.143
Limiting indices	$-58 \le h \le 58$	$-30 \le h \le 30$	$-30 \le h \le 30$	$-30 \le h \le 30$	$-18 \le h \le 18$
	$-54 \le k \le 58$	$-18 \le k \le 18$	$-18 \le k \le 18$	$-18 \le k \le 18$	$-15 \le k \le 15$
	$-11 \le l \le 11$	$-26 \le l \le 26$	$-26 \le l \le 26$	$-24 \le l \le 26$	$-33 \le l \le 43$
Reflns collected	73 132	105 509	103 059	93 668	127 695
Params	493	941	941	921	829
R_{int}	0.0668	0.0744	0.0457	0.0945	0.1138
GOF on F^2	1.068	1.053	1.039	1.077	1.062
R_1, wR_2 [$I > 2\sigma(I)$]	0.0415, 0.0988	0.0476, 0.1154	0.0450, 0.1119	0.0545, 0.1307	0.0944, 0.2244
R_1, wR_2 (all data)	0.0582, 0.1086	0.0774, 0.1358	0.0629, 0.1303	0.0961, 0.1563	0.1548, 0.2606

Table 2 Crystallographic data and structure refinements for clusters **6–10**

	6	**7**	**8**	**9**	**10**
Formula	$C_{64}H_{90}Dy_4N_6O_{26}$	$C_{78}H_{82}Er_6N_{12}O_{26}$	$C_{64}H_{90}N_6O_{26}Tm_4$	$C_{78}H_{84}N_{12}O_{26}Yb_6$	$C_{58}H_{66}Cl_4Lu_4N_6O_{20}$
*M*r (g mol^{-1})	2009.41	2607.11	2035.14	2643.81	2008.84
T (K)	150.0	150.0	150.01	150.0	150.0
Cryst syst	Monoclinic	Triclinic	Monoclinic	Monoclinic	Triclinic
Space group	$P2_1/c$	$P\bar{1}$	$P2_1/c$	$P2_1/c$	$P\bar{1}$
a (Å)	14.8441(11)	11.5180(9)	14.8499(11)	13.0254(7)	8.5600(4)
b (Å)	15.0331(10)	12.4304(9)	15.0852(12)	16.3691(10)	14.0982(7)
c (Å)	17.0783(13)	17.4525(12)	17.2237(13)	23.8144(14)	14.3191(6)
α (°)	90	104.453(4)	90	90	96.775(2)
β (°)	99.366(2)	98.872(4)	99.221(2)	101.522(2)	94.875(2)
γ (°)	90	109.749(3)	90	90	101.833(2)
V (Å^3)	18944(2)	2197.9(3)	3808.5(5)	4975.2(5)	1668.87(13)
Z	2	1	4	2	1
Cryst size (mm^3)	0.26 × 0.16 × 0.11	0.32 × 0.24 × 0.13	0.32 × 0.21 × 0.15	0.32 × 0.21 × 0.14	0.23 × 0.21 × 0.14
D_c (g cm^{-3})	1.775	1.970	1.775	1.765	1.999
μ (mm^{-1})	4.008	5.743	4.692	5.653	6.099
Limiting indices	$-18 \le h \le 18$	$-14 \le h \le 14$	$-18 \le h \le 18$	$-12 \le h \le 16$	$-10 \le h \le 10$
	$-18 \le k \le 18$	$-15 \le k \le 15$	$-18 \le k \le 18$	$-20 \le k \le 20$	$-17 \le k \le 17$
	$-21 \le l \le 21$	$-21 \le l \le 21$	$-21 \le l \le 21$	$-29 \le l \le 29$	$-17 \le l \le 17$
Reflns collected	50 379	38 257	64 590	74 897	31 259
Params	471	539	471	563	422
R_{int}	0.0890	0.1068	0.0853	0.0654	0.0453
GOF on F^2	1.078	1.020	1.030	1.052	1.040
R_1, wR_2 [$I > 2\sigma(I)$]	0.0463, 0.1072	0.0491, 0.1039	0.0567, 0.1439	0.0381, 0.0922	0.0291, 0.0656
R_1, wR_2 (all data)	0.0815, 0.1269	0.0926, 0.1208	0.0977, 0.1812	0.0546, 0.1032	0.0383, 0.0691

Fig. 3. The four central Dy ions are bridged by six μ_2-O atoms (O1, O2, O3, O1a, O2a and O3a) of two L^{2-} ligands, leading to an approximate linear-shaped Dy_4 arrangement with the Dy1···Dy2 distance of 3.9086(6) Å and Dy1···Dy1a distance of 3.8543(5) Å. The Dy2–Dy1–Dy1a angle is 129.632°, and the Dy–O–Dy angles are in the range of 109.042°–112.852°. The O–Dy–O angles in cluster **6** are in the range of 68.1317°–147.65(18)°. Furthermore, it is worth mentioning that the six μ_2-O atoms (O1, O2, O3, O1a, O2a and O3a) are bridged the four Dy ions forming three parallelogram-shaped Dy_2O_2 cores.

Crystal structures of clusters 7 and 9

Clusters **7** and **9** are isostructural, which was confirmed by the single-crystal structural measurement. Therefore, cluster **7** is selected as a detailed example. Cluster **7** crystallizes in the triclinic space group $P\bar{1}$ with $Z = 1$. As shown in Fig. 4, the mole-

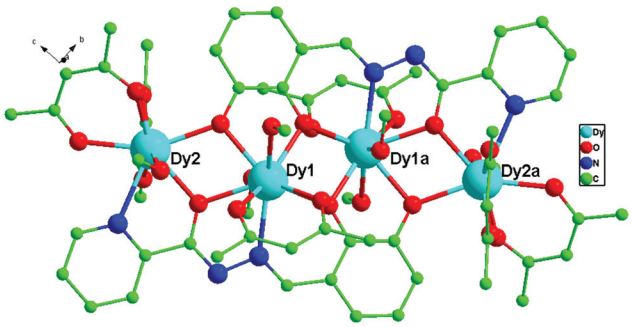

Fig. 1 Molecular structure for **6** (all hydrogen atoms are omitted for clarity).

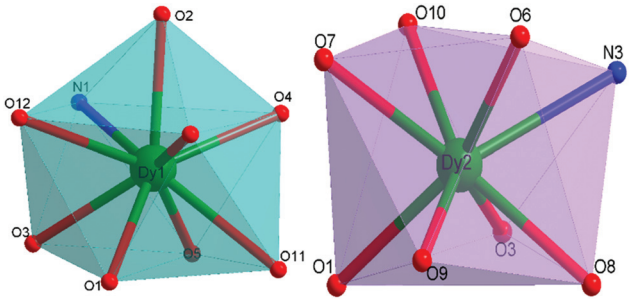

Fig. 2 (Left) Nine-coordinate distorted geometry around the Dy1 ion; (right) eight-coordinate distorted geometry around the Dy2 ion.

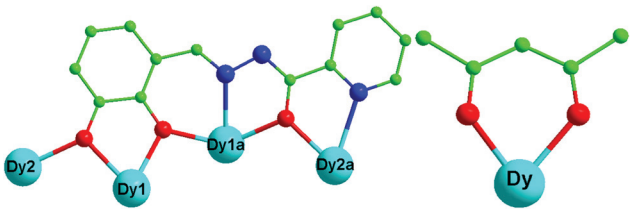

Fig. 3 Coordination modes of H_2L (left) and $acac^-$ (right) in **6** (green, C; red, O; blue, N; and turquoise, Dy).

cular structure of **7** mainly consists of six Er^{III} ions, four L^{2-}, six CH_3O^-, and four $acac^-$. In the asymmetric unit, both Er1 and Er2 ions are 8-coordinated. The Er1 ion is coordinated by one nitrogen atom (N1) and seven oxygen atoms (O1, O2, O3, O4, O5, O2a and O12) and the Er2 ion is connected by two nitrogen atoms (N3 and N4) and six oxygen atoms (O1, O3, O5, O6, O11 and O13) (Fig. S3†), while the central Er3 ion is seven-coordinated with a NO_6 coordination environment. The coordination polyhedrons of the central Er1 and Er2 atoms can be described as a distorted biaugmented trigonal prism geometry, and that of the coordination polyhedron of the central Er3 atom could be described as a distorted pentagonal bipyramid geometrical configuration (Fig. S4†), these are also confirmed by using the SHAPE 2.0 software (Table S1†). In **7**, the H_2L adopt two different coordination modes connected to the central Er1 ions, which is shown as Fig. S5.† The six central Er ions are connected by twelve μ_2-O atoms from four L^{2-} ligands and two CH_3O^-, leading to an approximate linear-shaped Er_6 arrangement. In the Er_6 core, the Er1···Er2 distance is 3.5064 Å, Er2···Er3 distance is 3.7515 Å, and Er1···Er1a distance is 3.6402 Å, the Er1–Er2–Er3 angle is 148.792° and Er1a–Er1–Er2 angle is 146.694°. In addition, the Er–O bond distances of **7** are in the range of 2.238(8)–2.389(6) Å, and the Er–N bond lengths are 2.417(8), 2.518(8) and 2.540(8) Å, respectively. The O–Er–O bond angles are in the range of 66.2(2)°–169.6(3)°. These bonds lengths and angles are comparable to those of the previously reported Ln_6 clusters in the literature.[29]

Crystal structures of cluster 10

The crystal structure of **10** is very similar to that of clusters **1–6** and **8**, as shown in Fig. 5. It mainly contains four Lu^{III} ions, six $acac^-$, two L^{2-} and two coordinated water molecules. Different from the structures of clusters **1–6** and **8**, the central Lu1(III) ion is seven-coordinated and Lu2(III) ion is eight-coordinated. The Lu1(III) ion is coordinated by one nitrogen atom (N1) form the ligand L^{2-} and six oxygen atoms (O1a, O3, O6, O7, O8 and O9) from two $acac^-$ and two L^{2-} ligands (Fig. S6†). The Lu2(III) ion is connected by one nitrogen atom (N3) and seven oxygen atoms (O1, O2, O4, O5, O10, O2a and O3a) with a NO_7 coordination environment. The coordination mode of H_2L in **10** is just the same as that in clusters **1–6** and **8** (Fig. S7†). The four central Lu(III) ions are bridged by six μ_2-O atoms from two L^{2-} ligands forming an approximate linear-shaped Lu_4 arrangement. In the Lu_4 core, the distances of the neighbouring Lu(III)

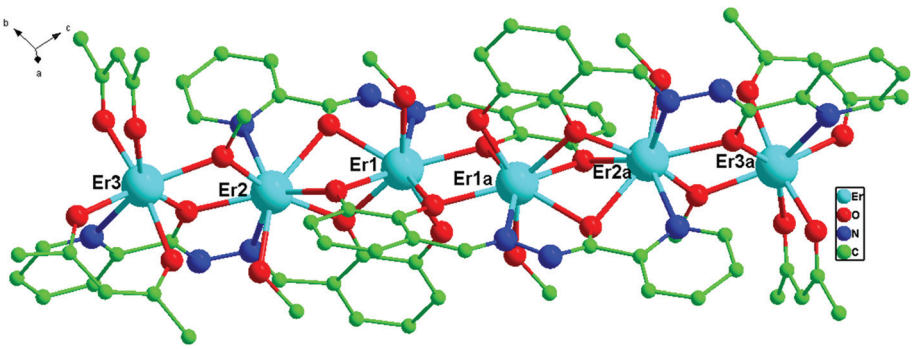

Fig. 4 Molecular structure for **7** (all hydrogen atoms are omitted for clarity).

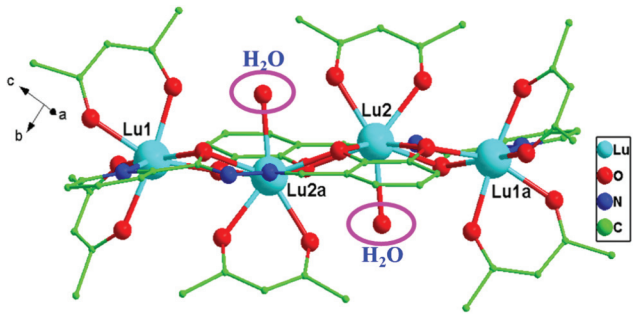

Fig. 5 Molecular structure for **10** (all hydrogen atoms are omitted for clarity).

ions are 3.6875(3) and 3.6974(4) Å, respectively. The Lu1–Lu2a–Lu2 angle is 139.432°, which is slightly larger than the Dy2–Dy1–Dy1a angle in **6**. Furthermore, in cluster **10**, the Lu–O bond distances are in the range of 2.214(4)–2.371(4) Å, and the Lu–N bond lengths are 2.372(4) and 2.494(5) Å, respectively. The O–Lu–O bond angles are in the range of 68.47(13)°–141.70(13)°.

Powder X-ray diffraction and TG analyses

To verify the purity of the crystal samples **1–10**, the powder XRD diffraction (PXRD) analyses of clusters **1–10** were carried out, and are shown in Fig. S8.† The experimental PXRD data of clusters **1–10** are almost identical to that of the corresponding simulated one, which suggests that the purities of the crystal samples **1–10** are high.

The thermogravimetric analyses (TGA) were performed in the temperature range of 40–800 °C under N_2 atmosphere to study the stability of clusters **1–10** (Fig. 6). The TGA curves of clusters **1–6**, **8** and **10** are very similar since they are isomorphic. Therefore, cluster **1** is selected as a representative illustration. Between 40 and 200 °C, a weight loss of 3.65% is observed, which corresponds to the loss of two CH_3OH molecules (calculated 3.27%). Subsequently, a weight loss of 31.60% occurs from 200 to about 490 °C, which is related to the loss of six coordinated acetylacetone molecules (calculated 30.63%). After that, cluster **1** decomposes gradually. For clusters **7** and **9**, their TGA curves also show a similar tendency; herein, we select the TGA curve of cluster **7** for describing in detail. In the range from 40 to 320 °C, the TGA curve displays a weight loss of 4.82% (calculated 4.91%), which is attributed to the loss of four coordinated methanol molecules. Then, a weight loss of 16.12% occurs between 320 and 400 °C, which corresponds to the loss of four acetylacetone molecules (calculated 15.34%). Subsequently, cluster **7** decomposes gradually in the temperature range of 400–800 °C.

UV–vis spectra

The UV–vis spectra of the multidentate Schiff base ligand ($\mathbf{H_2L}$) and clusters **1–10** were obtained in ethanol solution at room temperature (Fig. S9 in ESI†). For the multidentate Schiff base ligand ($\mathbf{H_2L}$), three absorption bands are clearly observed at *ca.* 206, 225, and 308 nm. The peak at *ca.* 206 nm can be attributed to the n → σ* transition; the observed strong peak at *ca.* 225 and 308 nm may be attributed to a π → π* transition of the aromatic rings in $\mathbf{H_2L}$. The UV–vis spectra of **1–10** display four similar absorption peaks. The absorption bands in the range 203–209 nm, 236–242 nm, and 296–303 nm result from the ligand $\mathbf{H_2L}$, and the absorption bands at about 345 nm are ascribed to the π → π* transition of $acac^-$. Compared with the $\mathbf{H_2L}$ ligand, the absorption peak range at 236–242 nm in clusters **1–10** is red shifted, and the absorption peak range at 296–303 nm is blue shifted, which may be due to the coordination effects of $acac^-$ and $\mathbf{H_2L}$ with the Ln(III) ion.

Fluorescence properties

The solid-state fluorescence properties of clusters **2**, **3**, **5** and **6** were measured at room temperature. As shown in Fig. 7, under excitation at 286 nm, three characteristic emission peaks of cluster **2** appear at 561, 596 and 643 nm, which are attributed to $^4G_{5/2} \rightarrow {}^6H_J$ (J = 5/2, 7/2, 9/2) transitions of Sm^{3+} ion, respectively. For **3**, under excitation at 290 nm, five characteristic emission peaks are observed at 546, 595, 616, 655 and 700 nm; these characteristic emission peaks are attributed to $^5D_1 \rightarrow {}^7F_1$ and $^5D_0 \rightarrow {}^7F_J$ (J = 1, 2, 3, 4) transitions of Eu^{3+} ion,

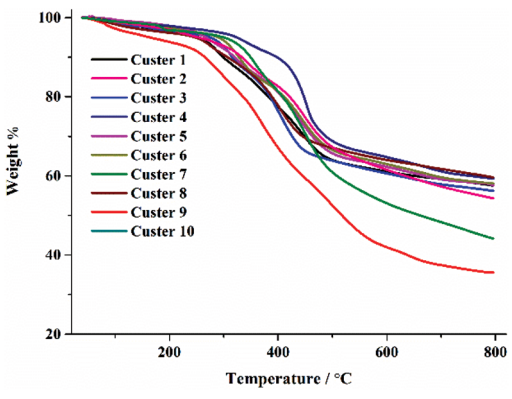

Fig. 6 The TGA curves of clusters **1–10**.

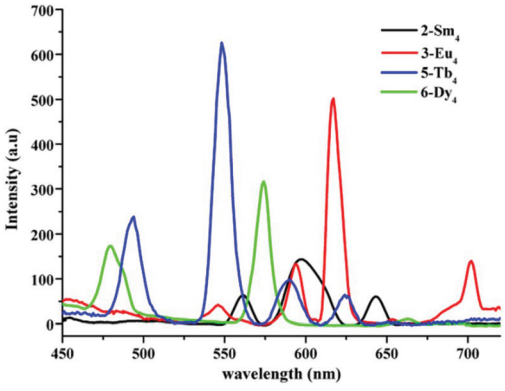

Fig. 7 The solid-state fluorescent spectra of **2**, **3**, **5** and **6** at room temperature.

respectively. These characteristic peaks are commonly observed in Eu(III)-based complexes.[30] Under the same excitation of 296 nm, the emission spectra of clusters **5** and **6** exhibit the characteristic emissions of Tb(III) and Dy(III) ions. For cluster **5**, four characteristic emission peaks are observed at 490, 545, 585 and 620 nm, corresponding to the transitions of Tb(III) ion from $^5D_4$ to ^7F_J (J = 6, 5, 4, 3), respectively; while for cluster **6**, two characteristic peaks of Dy(III) ion are observed, which belong to the transitions of $^4F_{9/2} \rightarrow {}^6H_{15/2}$ (480 nm) and $^4F_{9/2} \rightarrow {}^6H_{13/2}$ (576 nm). These characteristic peaks are usually observed in Tb(III) and Dy(III)-based compounds.[31]

Magnetic properties

Direct-current (dc) magnetic susceptibility studies of the polycrystalline samples for clusters **4–9** were performed in the temperature range of 300–2.0 K under a 1.0 kOe applied field. As shown in Fig. 8, at room-temperature, the $\chi_M T$ values of **4**, **5**, **6**, **7**, **8** and **9** are 31.59, 47.44, 56.89, 71.82, 28.82 and 15.60 cm^3 K mol^{-1}, respectively, which are near to those theoretically calculated based on four or six isolated Ln(III) ions: four uncoupled Gd(III) ions ($^8S_{7/2}$, g = 2) with the expected value of 31.52 cm^3 K mol^{-1} for **4**; four uncoupled free Tb(III) ions ($^7S_6$, g = 3/2) with the expected value of 47.28 cm^3 K mol^{-1} for **5**; four uncoupled Dy(III) ions ($^6H_{15/2}$, g = 4/3) with the expected value of 56.68 cm^3 K mol^{-1} for **6**; six uncoupled Er(III) ions ($^4I_{15/2}$, g = 6/5) with the expected value of 68.88 cm^3 K mol^{-1} for **7**; four uncoupled Tm(III) ions ($^3H_6$, g = 7/6) with the expected value of 28.60 cm^3 K mol^{-1} for **8**; and six uncoupled Yb(III) ions ($^2F_{7/2}$, g = 8/7) with the expected value of 15.18 cm^3 K mol^{-1} for **9**. For cluster **4**, the experimental $\chi_M T$ value is almost unchanged in the temperature range of 300–25 K; as the temperature further decreases, the $\chi_M T$ value drops quickly to a minimum value of 14.24 cm^3 K mol^{-1} at 2.0 K, which reveals the presence of a weak antiferromagnetic interaction between the Gd(III) ions in **4**.[32] For clusters **5–9**, $\chi_M T$ values decrease slowly in the temperature range of 300–20 K and then decrease distinctly to reach minima of 22.62, 31.02, 39.55, 15.31 and 7.96 cm^3 K mol^{-1} at 2.0 K, respectively. Such behaviors are usually due to the thermal depopulation of the Ln(III) Stark sublevels and/or the weak antiferromagnetic interactions between the adjacent Ln(III) ions in clusters **5–9**.[33]

Furthermore, in order to study the magnetic interactions between the adjacent Gd(III) ions in cluster **4**, the magnetic susceptibility of **4** was fitted to the Curie–Weiss law,[34] and the parameters θ = −2.99 K and C = 31.56 cm^3 K mol^{-1} (R = 0.99994) for **4** were obtained. The negative parameter θ of **4** further supports the occurrence of antiferromagnetic coupling between the adjacent Gd(III) ions (Fig. S10†).[35] Moreover, the $\chi_M T$ *vs.* T plot of cluster **4** can be fitted using the Hamiltonian (1), which is based on the model given in Fig. S11.† The well-fitted data of **4** give the parameters J = −0.09 cm^{-1} and g = 2.02 (R = 0.98528). The low and negative J value also indicates that a weak antiferromagnetic coupling between the adjacent Gd(III) ions exists in cluster **4**.[36]

$$H_{Gd_4} = -J(\mathrm{Gd1Gd2} + \mathrm{Gd1Gd1a} + \mathrm{Gd1aGd2a}) - g\mu_B H \cdot \sum_{i=1}^{4} \mathrm{Gd}i \quad (1)$$

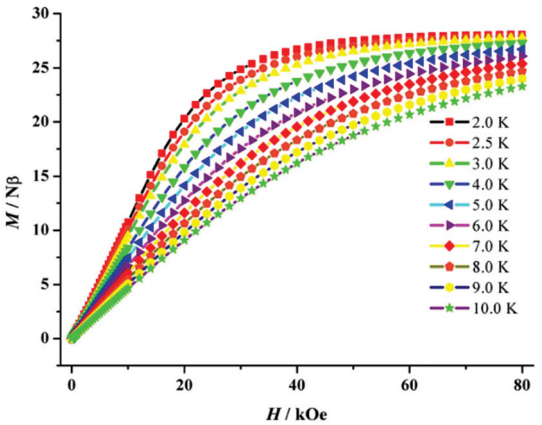

Fig. 9 Plots of M *vs.* H at the indicated temperatures for **4**.

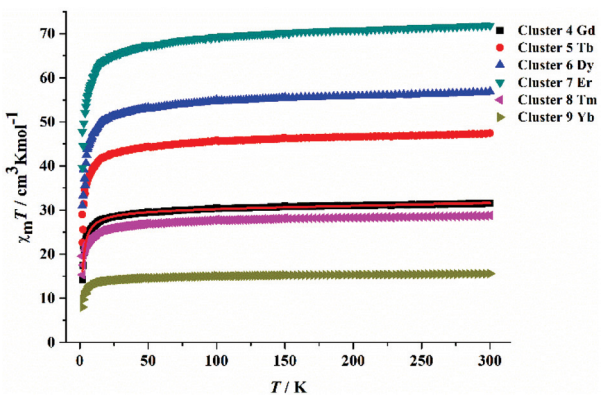

Fig. 8 Temperature dependence of the $\chi_M T$ products at 1000 Oe for clusters **4–9**, the red solid line is the best fit obtained for **4**.

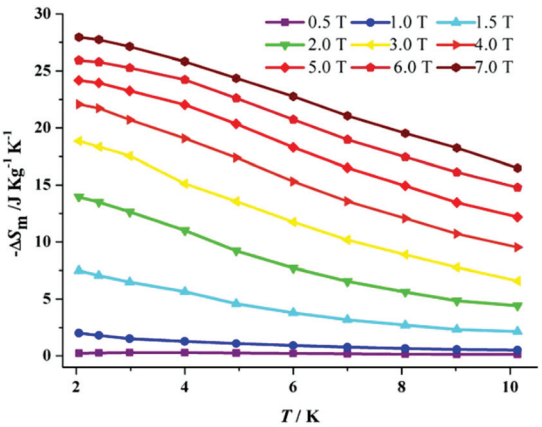

Fig. 10 Temperature dependencies (2.0–10.0 K) of $-\Delta S_m$ as obtained from magnetization data for **4**.

Table 3 Comparison of the $-\Delta S_m$ values among cluster **4** and recently reported Gd_4 clusters

Gd_4 compounds	Magnetic interaction	$-\Delta S_m$ (J kg^{-1} K^{-1}) (ΔH)	Ref.
$[Gd_4(HL)_4(\mu_2\text{-}CH_3O)_4]\cdot 4CH_3OH$	AF	34.46 (7 T)	17*a*
$[Gd_4(L)_2(dbm)_6(CH_3OH)_2]$	AF	21.39 (5 T)	18*b*
$[Gd_4(L)_2(dbm)_6(C_2H_5OH)_2]$	AF	20.26 (7 T)	18*b*
$[Gd_4(dbm)_4L_6(\mu_3\text{-}OH)_2]\cdot 5CH_3CN\cdot 0.5CH_2Cl_2$	AF	17.77 (7 T)	19*a*
$[Gd_4(acac)_4L_6(\mu_3\text{-}OH)_2]\cdot 2CH_3CN$	AF	22.11 (7 T)	19*a*
Cluster **4**	AF	27.96 (7 T)	This work
$[Gd_4(acac)_4L_6(\mu_3\text{-}OH)_2]\cdot CH_3CN\cdot 0.5CH_2Cl_2$	AF	25.08 (7 T)	19*b*
$[Gd_4(dbm)_4(L)_6(\mu_3\text{-}OH)_2]\cdot 5CH_3CN$	AF	16.35 (7 T)	19*e*
$[Gd_4(acac)_4L_6(\mu_3\text{-}OH)_2]$	AF	20.8 (7 T)	19*f*
$[Gd_4(acac)_4(\mu_3\text{-}OH)_2(L)_6]\cdot 4CH_3CN$	AF	23.37 (7 T)	19*g*
$[Gd_4(\mu_3\text{-}OH)_2L_6(acac)_4]\cdot 2CH_3CN$	AF	18.85 (7 T)	28*a*
$\{[Gd_4(L)_6(pbd)_4(\mu_3\text{-}OH)_2]\cdot 2CH_3CN\}$	AF	21.42 (7 T)	28*b*
$[Gd_4(L)_6(tmhd)_4(\mu_3\text{-}OH)_2]$	AF	20.85 (7 T)	28*c*
$[Gd_4(\mu_3\text{-}OH)_2(tmhd)_4L_6]\cdot 2CH_3CN$	AF	17.94 (7 T)	30*b*
$[Gd_4(\mu_3\text{-}OH)_2L_6(acac)_4]\cdot 2.5CH_3CN$	AF	19.39 (7 T)	33*c*
$[Gd_4(\mu_3\text{-}OH)_2L_6(tmhd)_4]\cdot CH_3CN\cdot CH_3CH_2OH$	AF	16.21 (7 T)	33*c*
$[Gd_4(CO_3)(L)_4(acac)_2(H_2O)_4]\cdot 2CH_3CN$	AF	31.23 (7 T)	42*c*
$[Gd_4CO_3L_4(acac)_2(MeOH)_2(H_2O)_2]\cdot MeOH\cdot H_2O$	AF	27.06 (7 T)	42*c*

In view of the important magnetic isotropy of Gd(III) ions, cluster **4** may be a good candidate for magnetocaloric materials. Hence, the magnetization data of cluster **4** was measured in the temperature range of 2.0–10.0 K under a field of 0–80 kOe. As shown in Fig. 9, with the increasing magnetic field, the *M vs. H* plots display a steady increase and a complete saturation value of $28.05N\beta$ is obtained at 2.0 K and 80 kOe, which is approximately close to the theoretical value of $28.0N\beta$ for four free Gd(III) ($S = 7/2$, $g = 2$) ions. The magnetic entropy changes ($-\Delta S_m$) of cluster **4** are calculated from the *M vs. H* data to evaluate the MCE, which is calculated by using the Maxwell equation: $\Delta S_m(T) = \int [\partial M(T,H)/\partial T]_H dH$.[37] According to the Maxwell equation, the $-\Delta S_m$ values of **4** were obtained, and the curves of $-\Delta S_m$ *vs.* T are shown in Fig. 10. The maximum value of $-\Delta S_m$ is 27.96 J K^{-1} kg^{-1} under the field change $\Delta H = 7.0$ T and $T = 2.0$ K, which is smaller than the expected maximum $-\Delta S_m$ (34.78 J K^{-1} kg^{-1}, calculated as $4R\ln(2S + 1)$, where R is the gas constant and $S = 7/2$ for Gd(III) ion). The significant divergence for maximum $-\Delta S_m$ between the experimental and theoretical values of cluster **4** is mainly due to the antiferromagnetic interaction between the Gd(III) ions in **4**.[38] By comparison, cluster **4** has a large magnetic entropy change ($-\Delta S_m$) compared with the recently reported Gd_4 compounds as magnetocaloric materials, which is summarized in Table 3. Among all the reported Gd_4 molecule magnetic cooling materials, only a few compounds have a maximum $-\Delta S_m$ of above 30.0 J kg^{-1} K^{-1}. Therefore, cluster **4** is a possible magnetic refrigerant to be used in practice.

Meanwhile, considering the large magnetic anisotropy associated with Tb(III) and Dy(III) ions and in order to probe the dynamic behavior in clusters **5** and **6**, in the temperature range of 2.0–20 K, alternating current (ac) magnetic susceptibility measurement was undertaken at 3.0 Oe ac field and varying the frequency from 111 to 2311 Hz (Fig. S12† and Fig. 11). For **6**, the result revealed that the out-of-phase (χ'') ac magnetic susceptibility signals show a frequency dependence under zero dc field and obvious peaks were observed in the out-of-phase (χ'') signals, revealing the occurrence of a slow relaxation behavior in **6**;[39] however, no out-of-phase (χ'') alternating current (ac) signals were noticed for cluster **5**. To further deeply study the dynamic behavior of **6**, the frequency dependence of ac susceptibility was measured. As shown in

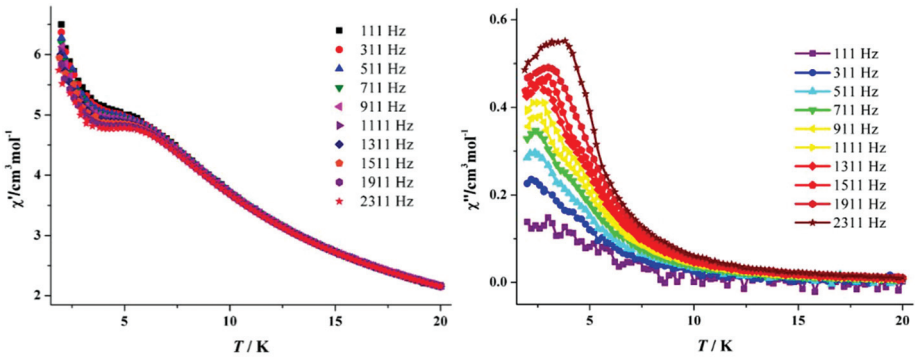

Fig. 11 Temperature dependence of the in-phase (left) and out-of-phase (right) components of the ac magnetic susceptibility for **6** in zero dc field with an oscillation of 3.0 Oe.

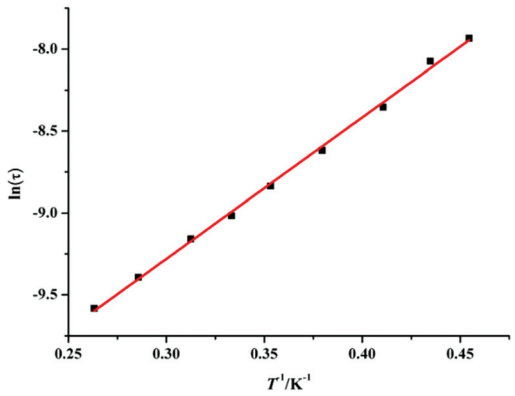

Fig. 12 ln τ *versus* T^{-1} plot for **6** under zero dc fields. The red solid line represents the least-squares fits of the experimental data to the Arrhenius law.

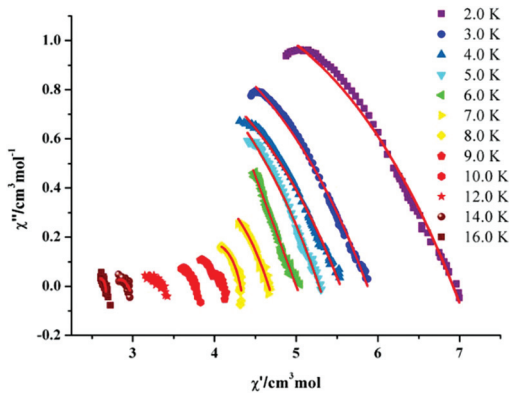

Fig. 13 Cole–Cole plots for **6** measured in zero-dc field. The solid lines are the best fit to the experimental data, obtained with the generalized Debye model with α = 0.07–0.17.

Fig. S13,† the out-of-phase (χ'') signals of the ac susceptibility of **6** show temperature dependences, which further confirms the SMM behavior in **6**.[40] The relaxation time τ data derived from the out-of-phase (χ'') peaks can be fitted by the Arrhenius law: $\tau = \tau_0 \exp(\Delta E/k_B T)$.[41] As shown in Fig. 12, the best fitting results obtained the effective energy barrier ($\Delta E/k_B$) of 8.64 K and the pre-exponential factor (τ_0) of 6.98×10^{-6} s. The obtained values of $\Delta E/k_B$ and τ_0 fall into the normal range of the already reported Dy_4 SMMs.[42]

The Cole–Cole diagrams of χ'' *vs.* χ' for cluster **6** show asymmetric semicircle shapes and were fitted to the generalized Debye model to obtain α values.[43] As shown in Fig. 13, α = 0.07–0.17 is obtained in the temperature range of 2.0–16.0 K, the small α values imply that a narrower relaxation distribution occurs in **6**.

Conclusion

In summary, a series of new linear-shaped Ln_4^{III} and Ln_6^{III} clusters which are constructed by a polydentate Schiff base ligand H_2L and acetylacetone co-ligand have been obtained. The crystal structures, luminescent properties and magnetic properties of these Ln_4^{III} and Ln_6^{III} clusters have been studied systematically. The investigations on the luminescent properties reveal that clusters **2**, **3**, **5** and **6** display the characteristic lanthanum luminescence at room temperature. Magnetic studies illustrate that cluster **4** exhibits significant MCE with a larger $-\Delta S_m$ value of 27.96 J kg^{-1} K^{-1} at 2.0 K and 7.0 T, indicating that cluster **4** is a potential magnetic refrigerant. Meanwhile, cluster **6** displays SMM behaviors under zero dc field with the effective energy barrier $\Delta E/k_B$ = 8.64 K and $\tau_0 = 6.98 \times 10^{-6}$ s.

Conflicts of interest

There are no conflicts to declare.

Acknowledgements

This work was supported financially by the Scientific and Technological Innovation Programs of Higher Education Institutions in Shanxi (No. 201802099), and the National Natural Science Foundation of China (21571138).

Notes and references

1 (*a*) K. Liu, X. J. Zhang, X. X. Meng, W. Shi, P. Cheng and A. K. Powell, *Chem. Soc. Rev.*, 2016, **45**, 2423; (*b*) P. Zhang, Y. N. Guo and J. K. Tang, *Coord. Chem. Rev.*, 2013, **257**, 1728; (*c*) J. Long, Y. Guari, R. A. S. Ferreira, L. D. Carlos and J. Larionova, *Coord. Chem. Rev.*, 2018, **363**, 57; (*d*) X. L. Li and J. K. Tang, *Dalton Trans.*, 2019, **48**, 15358.

2 (*a*) Y. Z. Zheng, G. J. Zhou, Z. P. Zheng and R. E. P. Winpenny, *Chem. Soc. Rev.*, 2014, **43**, 1462; (*b*) A. Rasamsetty, C. Das, E. C. Sañudo, M. Shanmugam and V. Baskar, *Dalton Trans.*, 2018, **47**, 1726; (*c*) K. Wang, Z. L. Chen, H. H. Zou, S. H. Zhang, Y. Li, X. Q. Zhang, W. Y. Sun and F. P. Liang, *Dalton Trans.*, 2018, **47**, 2337; (*d*) S. J. Liu, S. D. Han, J. P. Zhao, J. L. Xu and X. H. Bu, *Coord. Chem. Rev.*, 2019, **394**, 39; (*e*) M. Kumar, L. H. Wu, M. Kariem, A. Franconetti, H. N. Sheikh, S. J. Liu, S. C. Sahoo and A. Frontera, *Inorg. Chem.*, 2019, **58**, 7760; (*f*) S. W. Zhang and P. Cheng, *Chem. Rec.*, 2016, **16**, 2077.

3 (*a*) S. V. Eliseeva and J. C. G. Bünzli, *Chem. Soc. Rev.*, 2010, **39**, 189; (*b*) J. Liu, A. M. Kaczmarek and R. V. Deun, *Chem. Soc. Rev.*, 2018, **47**, 7225; (*c*) Y. J. Cui, J. Zhang, H. J. He and G. D. Qian, *Chem. Soc. Rev.*, 2018, **47**, 5740; (*d*) J. Dong, H. Xu, S. L. Hou, Z. L. Wu and B. Zhao, *Inorg. Chem.*, 2017, **56**, 6244; (*e*) J. Y. Zou, L. Li, S. Y. You, Y. W. Liu, H. M. Cui, J. Z. Cui and S. W. Zhang, *Dalton Trans.*, 2018, **47**, 15694.

4 (*a*) J. Qin, P. Wang, Q. Y. Li, Y. Zhang, D. Yuan and Y. M. Yao, *Chem. Commun.*, 2014, **50**, 10952; (*b*) H. Xu, B. Zhai, C. S. Cao and B. Zhao, *Inorg. Chem.*, 2016, **55**,

9671; (*c*) J. Dong, P. Cui, P. F. Shi, P. Cheng and B. Zhao, *J. Am. Chem. Soc.*, 2015, **137**, 15988.

5 (*a*) J. D. Rinehart and J. R. Long, *Chem. Sci.*, 2011, **2**, 2078; (*b*) L. Spree and A. A. Popov, *Dalton Trans.*, 2019, **48**, 2861; (*c*) J. W. Zhang, Y. Man, W. H. Liu, B. Q. Liu and Y. P. Dong, *Dalton Trans.*, 2019, **48**, 2560; (*d*) D. D. Yin, Q. Chen, Y. S. Meng, H. L. Sun, Y. Q. Zhang and S. Gao, *Chem. Sci.*, 2015, **6**, 3095; (*e*) W. M. Wang, S. Y. Wang, H. X. Zhang, H. Y. Shen, J. Y. Zou, H. L. Gao, J. Z. Cui and B. Zhao, *Inorg. Chem. Front.*, 2016, **3**, 133.

6 (*a*) L. Bogani, C. Sangregorio, R. Sessoliand and D. Gatteschi, *Angew. Chem., Int. Ed.*, 2005, **44**, 5817; (*b*) J. M. Zadroany and J. R. Long, *J. Am. Chem. Soc.*, 2011, **133**, 20732.

7 N. Ishikawa, M. Sugita, T. Ishikawa, S. Y. Koshihara and Y. Kaizu, *J. Am. Chem. Soc.*, 2003, **125**, 8694.

8 (*a*) Z. F. Yang, Y. M. Tian, W. Y. Zhang, P. Chen, H. F. Li, Y. Q. Zhang and W. B. Sun, *Dalton Trans.*, 2019, **48**, 4931; (*b*) S. Biswas, P. Kumar, A. Swain, T. Gupta, P. Kalita, S. Kundu, G. Rajaraman and V. Chandrasekhar, *Dalton Trans.*, 2019, **48**, 6421; (*c*) G. Peng, Y. Y. Zhang, B. Li, X. F. Sun, H. L. Cai, D. J. Li, Z. G. Gu and G. E. Kostakis, *Dalton Trans.*, 2018, **47**, 17349; (*d*) K. Zhang, G. P. Li, V. Montigaud, O. Cador, B. L. Guennic, J. K. Tang and Y. Y. Wang, *Dalton Trans.*, 2019, **48**, 2135; (*e*) K. Zhang, G. P. Li, C. Zhang and Y. Y. Wang, *Dalton Trans.*, 2019, **48**, 5793.

9 (*a*) S. K. Gupta, T. Rajeshkumar, G. Rajaraman and R. Murugavel, *Chem. Sci.*, 2016, **7**, 5181; (*b*) J. Xiong, H. Y. Ding, Y. S. Meng, C. Gao, X. J. Zhang, Z. S. Meng, Y. Q. Zhang, W. Shi, B. W. Wang and S. Gao, *Chem. Sci.*, 2017, **8**, 1288; (*c*) J. Liu, Y. C. Chen, J. L. Liu, V. Vieru, L. Ungur, J. H. Jia, L. F. Chibotaru, Y. Lan, W. Wernsdorfer, S. Gao, X. M. Chen and M. L. Tong, *J. Am. Chem. Soc.*, 2016, **138**, 5441; (*d*) Y. S. Ding, N. F. Chilton, R. E. P. Winpenny and Y. Z. Zheng, *Angew. Chem., Int. Ed.*, 2016, **55**, 16071; (*e*) F. S. Guo, B. M. Day, Y. C. Chen, M. L. Tong, A. Mansikkamäki and R. A. Layfield, *Angew. Chem., Int. Ed.*, 2017, **56**, 11445; (*f*) C. A. P. Goodwin, F. Ortu, D. Reta, N. F. Chilton and D. P. Mills, *Nature*, 2017, **548**, 439; (*g*) S. W. Zhang, H. Li, E. Y. Duan, Z. S. Han, L. L. Li, J. K. Tang, W. Shi and P. Cheng, *Inorg. Chem.*, 2016, **55**, 1202.

10 X. Y. Zheng, J. Xie, X. J. Kong, L. S. Long and L. S. Zheng, *Coord. Chem. Rev.*, 2019, **378**, 222.

11 (*a*) J. L. Liu, Y. C. Chen and M. L. Tong, *Chem. Soc. Rev.*, 2018, **47**, 243; (*b*) Z. H. Zhu, M. Guo, X. L. Li and J. K. Tang, *Coord. Chem. Rev.*, 2019, **378**, 350.

12 J. L. Liu, Y. C. Chen, F. S. Guo and M. L. Tong, *Coord. Chem. Rev.*, 2014, **281**, 26.

13 (*a*) Z. M. Zhang, K. H. Zangana, A. K. Kostopoulos, M. L. Tong and R. E. P. Winpenny, *Dalton Trans.*, 2016, **45**, 9041; (*b*) M. Evangelisti, O. Roubeau, E. Palacios, A. Camon, T. N. Hooper, E. K. Brechin and J. J. Alonso, *Angew. Chem., Int. Ed.*, 2011, **50**, 6606; (*c*) R. Sessoli, *Angew. Chem., Int. Ed.*, 2012, **51**, 43; (*d*) S. W. Zhang and P. Cheng, *ChemPlusChem*, 2016, **81**, 811; (*e*) S. J. Liu, S. L. Yao, C. Cao, T. F. Zheng, C. Liu, Z. X. Wang, Q. Zhao, J. S. Liao, J. L. Chen and H. R. Wen, *Polyhedron*, 2017, **121**, 180.

14 (*a*) J. Z. Qiu, Y. C. Chen, L. F. Wang, Q. W. Li, M. Orendáč and M. L. Tong, *Inorg. Chem. Front.*, 2016, **3**, 150; (*b*) Y. C. Chen, L. Qin, Z. S. Meng, D. F. Yang, C. Wu, Z. D. Fu, Y. Z. Zheng, J. L. Liu, R. Tarasenko, M. Orendáč, J. Prokleška, V. Sechovský and M. L. Tong, *J. Mater. Chem. A*, 2014, **2**, 9851; (*c*) T. F. Zheng, C. Cao, P. P. Dong, S. J. Liu, F. F. Wang, X. L. Tong, J. S. Liao, J. L. Chen and H. R. Wen, *Polyhedron*, 2016, **113**, 96.

15 (*a*) Y. L. Hou, G. Xiong, P. F. Shi, R. R. Cheng, J. Z. Cui and B. Zhao, *Chem. Commun.*, 2013, **49**, 6066; (*b*) X. Y. Zheng, Y. H. Jiang, G. L. Zhuang, D. P. Liu, H. G. Liao, X. J. Kong, L. S. Long and L. S. Zheng, *J. Am. Chem. Soc.*, 2017, **139**, 18178; (*c*) Y. C. Chen, J. Prokleška, W. J. Xu, J. L. Liu, J. Liu, W. X. Zhang, J. H. Jia, V. Sechovský and M. L. Tong, *J. Mater. Chem. C*, 2015, **3**, 12206; (*d*) J. B. Peng, Q. C. Zhang, X. J. Kong, Y. Z. Zheng, Y. P. Ren, L. S. Long, R. B. Huang, L. S. Zheng and Z. P. Zheng, *J. Am. Chem. Soc.*, 2012, **134**, 3314; (*e*) S. J. Liu, C. Cao, C. C. Xie, T. F. Zheng, X. L. Tong, J. S. Liao, J. L. Chen, H. R. Wen, Z. Chang and X. H. Bu, *Dalton Trans.*, 2016, **45**, 9209; (*f*) S. J. Liu, C. Cao, S. L. Yao, T. F. Zheng, Z. X. Wang, C. Liu, J. S. Liao, J. L. Chen, Y. W. Li and H. R. Wen, *Dalton Trans.*, 2017, **46**, 64; (*g*) T. F. Zheng, S. L. Yao, C. Cao, S. J. Liu, H. K. Hu, T. Zhang, H. P. Huang, J. S. Liao, J. L. Chen and H. R. Wen, *New J. Chem.*, 2017, **41**, 8598; (*h*) S. W. Zhang, W. Shi and P. Cheng, *Coord. Chem. Rev.*, 2017, **352**, 108.

16 (*a*) Y. Z. Zheng, M. Evangelisti, F. Tuna and R. E. P. Winpenny, *J. Am. Chem. Soc.*, 2012, **134**, 1057; (*b*) J. B. Peng, X. J. Kong, Q. C. Zhang, M. Orenda, J. Prokleška, Y. P. Ren, L. S. Long, Z. P. Zheng and L. S. Zheng, *J. Am. Chem. Soc.*, 2014, **136**, 17938.

17 (*a*) W. M. Wang, X. Z. Li, L. Zhang, J. L. Chen, J. H. Wang, Z. L. Wu and J. Z. Cui, *New J. Chem.*, 2019, **43**, 7419; (*b*) M. U. Anwar, L. K. Thompson, L. N. Dawe, F. Habibb and M. Murugesu, *Chem. Commun.*, 2012, **48**, 4576; (*c*) A. Gusev, R. Herchel, I. Nemec, V. Shul'gin, I. L. Eremenko, K. Lyssenko, W. Linert and Z. Trávníček, *Inorg. Chem.*, 2016, **55**, 12470; (*d*) W. Huang, F. X. Shen, S. Q. Wu, L. Liu, D. Y. Wu, Z. Zheng, J. Xu, M. Zhang, X. C. Huang, J. Jiang, F. F. Pan, Y. Li, K. Zhu and O. Sato, *Inorg. Chem.*, 2016, **55**, 5476; (*e*) S. F. Xue, L. Zhao, Y. N. Guo, X. H. Chen and J. K. Tang, *Chem. Commun.*, 2012, **48**, 7031.

18 (*a*) R. X. Zhang, Y. X. Chang, H. Y. Shen, W. M. Wang, X. P. Zhou, N. N. Wang, J. Z. Cui and H. L. Gao, *Dalton Trans.*, 2016, **45**, 19117; (*b*) Y. C. Zhang, Q. L. Wang, G. Chen, P. F. Shi and W. M. Wang, *Polyhedron*, 2019, **169**, 247.

19 (*a*) H. L. Gao, N. N. Wang, W. M. Wang, H. Y. Shen, X. P. Zhou, Y. X. Chang, R. X. Zhang and J. Z. Cui, *Inorg. Chem. Front.*, 2017, **4**, 860; (*b*) H. L. Gao, X. P. Zhou, Y. X. Bi, H. Y. Shen, W. M. Wang, N. N. Wang, Y. X. Chang,

R. X. Zhang and J. Z. Cui, *Dalton Trans.*, 2017, **46**, 4669; (*c*) Z. L. Wu, Y. G. Ran, X. Y. Wu, Y. P. Xia, M. Fang and W. M. Wang, *Polyhedron*, 2017, **126**, 282; (*d*) X. X. Wang, X. R. Han, X. Si, M. Fang, W. M. Wang, H. K. Peng and M. Fang, *Polyhedron*, 2017, **137**, 306; (*e*) H. L. Gao, S. X. Huang, X. P. Zhou, Z. Liu and J. Z. Cui, *Dalton Trans.*, 2018, **47**, 3503; (*f*) H. L. Gao, L. Jiang, S. Liu, H. Y. Shen, W. M. Wang and J. Z. Cui, *Dalton Trans.*, 2016, **45**, 253; (*g*) W. M. Wang, L. Zhang, X. Z. Li, L. Y. He, X. X. Wang, Y. Shi, J. Wang, J. Dong and Z. L. Wu, *New J. Chem.*, 2019, **43**, 12941.

20 K. H. Zangana, E. M. Pineda and R. E. P. Winpenny, *Dalton Trans.*, 2014, **43**, 17101.

21 (*a*) B. H. Koo, K. S. Lim, D. W. Ryu, W. R. Lee, E. K. Koh and C. S. Hong, *Dalton Trans.*, 2013, **42**, 7204; (*b*) P. H. Guo, Y. Meng, Y. C. Chen, Q. W. Li, B. Y. Wang, J. D. Leng, D. H. Bao, J. H. Jia and M. L. Tong, *J. Mater. Chem. C*, 2014, **2**, 8858.

22 S. F. Xue, Y. N. Guo, L. Zhao, P. Zhang and J. K. Tang, *Dalton Trans.*, 2014, **43**, 1564.

23 R. J. Holmberg, C. J. Kuo, B. Gabidullin, C. W. Wang, R. Clérac, M. Murugesu and P. H. Lin, *Dalton Trans.*, 2016, **45**, 16769.

24 X. L. Li, J. F. Wu, J. K. Tang, B. L. Guennic, W. Shi and P. Cheng, *Chem. Commun.*, 2016, **52**, 9570.

25 S. F. Xue, L. Zhao, Y. N. Guo, P. Zhang and J. K. Tang, *Chem. Commun.*, 2012, **48**, 8946.

26 S. Katagiri, Y. Tsukahara, Y. Hasegawa and Y. Wada, *Bull. Chem. Soc. Jpn.*, 2007, **80**, 1492.

27 G. M. Sheldrick, *SHELX-97*, University of Gottingen, 1997.

28 (*a*) W. M. Wang, T. L. Han, Y. L. Shao, X. Y. Qiao, Z. L. Wu, Q. L. Wang, P. F. Shi, H. L. Gao and J. Z. Cui, *New J. Chem.*, 2018, **42**, 14949; (*b*) H. Yu, J. X. Yang, J. Q. Han, P. F. Li, Y. L. Hou, W. M. Wang and M. Fang, *New J. Chem.*, 2019, **43**, 8067; (*c*) M. Fang, L. J. Shao, T. X. Shi, Y. Y. Chen, H. Yu, P. F. Li, W. M. Wang and B. Zhao, *New J. Chem.*, 2018, **42**, 11847; (*d*) V. Chandrasekhar, S. Hossain, S. Das, S. Biswas and J. P. Sutter, *Inorg. Chem.*, 2013, **52**, 6346.

29 (*a*) Y. Z. Tong, Q. L. Wang, G. Yang, G. M. Yang, S. P. Yan, D. Z. Liao and P. Cheng, *CrystEngComm*, 2010, **12**, 543; (*b*) S. K. Langley, B. Moubaraki, C. M. Forsyth, I. A. Gassa and K. S. Murray, *Dalton Trans.*, 2010, **39**, 1705; (*c*) A. Baniodeh, N. Magnani, S. Bräse, C. E. Ansonb and A. K. Powell, *Dalton Trans.*, 2015, **44**, 6343.

30 (*a*) Y. L. Hou, G. Xiong, B. Shen, B. Zhao, Z. Chen and J. Z. Cui, *Dalton Trans.*, 2013, **42**, 3587; (*b*) Y. X. Zhang, Y. H. Zhang, B. Y. Liu, W. M. Wang, G. P. Tang, H. Y. Wei and Z. L. Wu, *New J. Chem.*, 2018, **42**, 18305.

31 (*a*) W. M. Wang, H. X. Zhang, S. Y. Wang, H. Y. Shen, H. L. Gao, J. Z. Cui and B. Zhao, *Inorg. Chem.*, 2015, **54**, 10610; (*b*) X. J. Che, S. L. Hou, Y. Shi, G. L. Yang, Y. L. Hou and B. Zhao, *Dalton Trans.*, 2019, **48**, 3453.

32 (*a*) A. K. Mondal, H. S. Jena, A. Malviya and S. Konar, *Inorg. Chem.*, 2016, **55**, 5237; (*b*) V. Chandrasekhar, S. Das, A. Dey, S. Hossain and J. P. Sutter, *Inorg. Chem.*, 2013, **52**, 11956; (*c*) W. M. Wang, Q. Wang, L. Bai, H. Qiao, X. Y. Zhao, M. Xu, S. Y. Liu, Y. Shi, M. Fang and Z. L. Wu, *Polyhedron*, 2018, **142**, 43; (*d*) W. M. Wang, Y. X. Zhang, J. C. Zhao, X. H. Zhang, Y. Tan, Y. Y. Cui, Y. Shi and Z. L. Wu, *Polyhedron*, 2018, **146**, 161; (*e*) W. M. Wang, X. F. Guan, X. D. Liu, M. Fang, C. F. Zhang, M. Fang and Z. L. Wu, *Inorg. Chem. Commun.*, 2017, **79**, 8.

33 (*a*) X. L. Li, J. F. Wu, L. Zhao, W. Shi, P. Cheng and J. K. Tang, *Chem. Commun.*, 2017, **53**, 3026; (*b*) T. Lacelle, G. Brunet, A. Pialat, R. J. Holmberg, Y. Lan, B. Gabidullin, I. Korobkov, W. Wernsdorfer and M. Murugesu, *Dalton Trans.*, 2017, **46**, 2471; (*c*) Y. X. Zhang, M. Li, B. Y. Liu, Z. L. Wu, H. Y. Wei and W. M. Wang, *RSC Adv.*, 2017, **7**, 55523; (*d*) T. F. Zheng, X. M. Tian, S. L. Yao, C. Cao, J. B. Cai and S. J. Liu, *J. Mol. Struct.*, 2018, **1165**, 326; (*e*) Y. X. Chang, F. Hou, M. Y. Feng, H. H. Zhang, T. T. Kang, W. M. Wang and M. Fang, *Inorg. Chim. Acta*, 2019, **486**, 83.

34 (*a*) W. M. Wang, W. Z. Qiao, H. X. Zhang, S. Y. Wang, Y. Y. Nie, H. M. Chen, Z. Liu, H. L. Gao, J. Z. Cui and B. Zhao, *Dalton Trans.*, 2016, **45**, 8182; (*b*) W. M. Wang, W. W. Duan, L. C. Yue, Y. L. Wang, W. Y. Ji, C. F. Zhang, M. Fang and Z. L. Wu, *Inorg. Chim. Acta*, 2017, **466**, 145.

35 (*a*) X. F. Guan, W. Y. Hou, X. Y. Qiao, Z. Q. Zhang, K. X. Liu, W. M. Wang, Y. Shi and F. Pan, *Inorg. Chim. Acta*, 2019, **484**, 47; (*b*) S. W. Zhang, W. Shi, L. L. Li, E. Y. Duan and P. Cheng, *Inorg. Chem.*, 2014, **53**, 10340.

36 O. Tegus, E. Bruck, K. H. J. Buschow and F. R. de Boer, *Nature*, 2002, **415**, 150.

37 (*a*) G. Xiong, X. Y. Qin, P. F. Shi, Y. L. Hou, J. Z. Cui and B. Zhao, *Chem. Commun.*, 2014, **50**, 4255; (*b*) L. X. Chang, G. Xiong, L. Wang, P. Cheng and B. Zhao, *Chem. Commun.*, 2013, **49**, 1055; (*c*) Y. S. Xue, T. T. Kang, H. H. Zhang, X. Y. Qiao, W. Y. Hou, F. Pan and W. M. Wang, *Polyhedron*, 2018, **154**, 480.

38 (*a*) Y. S. Xue, H. Qiao, X. Y. Zhao, S. Y. Liu, M. Xu, L. Bai and W. M. Wang, *Polyhedron*, 2018, **147**, 126; (*b*) L. Liu, C. Z. Cai, R. F. Wu, Y. Q. Zhang, C. G. Li, Y. P. Zhang, J. J. Wang and W. M. Wang, *Polyhedron*, 2019, **158**, 365; (*c*) S. J. Liu, T. F. Zheng, J. Bao, P. P. Dong, J. S. Liao, J. L. Chen, H. R. Wen, J. Xu and X. H. Bu, *New J. Chem.*, 2015, **39**, 6970; (*d*) S. L. Yao, C. Cao, X. M. Tian, T. F. Zheng, S. J. Liu, X. L. Tong, J. S. Liao, J. L. Chen and H. R. Wen, *ChemistrySelect*, 2017, **2**, 10673.

39 (*a*) P. H. Lin, T. J. Burchell, L. Ungur, L. F. Chibotaru, W. Wernsdorfer and M. Murugesu, *Angew. Chem., Int. Ed.*, 2009, **48**, 9489; (*b*) P. H. Guo, J. Liu, Z. H. Wu, H. Yan, Y. C. Chen, J. H. Jia and M. L. Tong, *Inorg. Chem.*, 2015, **54**, 8087; (*c*) S. J. Liu, Y. Cui, W. C. Song, Q. L. Wang and X. H. Bu, *Chin. J. Inorg. Chem.*, 2015, **31**, 1894; (*d*) R. P. Li, Q. Y. Liu, Y. L. Wang, C. M. Liu and S. J. Liu, *Inorg. Chem. Front.*, 2017, **4**, 1149.

40 (*a*) Y. N. Guo, G. F. Xu, P. Gamez, L. Zhao, S. Y. Lin, R. P. Deng, J. K. Tang and H. J. Zhang, *J. Am. Chem. Soc.*, 2010, **132**, 8538; (*b*) H. L. Gao, L. Jiang, S. Liu, H. Y. Shen, W. M. Wang and J. Z. Cui, *Dalton Trans.*, 2016, **45**, 253;

(*c*) W. M. Wang, X. M. Kang, H. Y. Shen, Z. L. Wu, H. L. Gao and J. Z. Cui, *Inorg. Chem. Front.*, 2018, **5**, 1876.

41 (*a*) M. Guo, Y. Q. Zhang, Z. H. Zhu and J. K. Tang, *Inorg. Chem.*, 2018, **57**, 12213; (*b*) Y. Zhang, B. Ali, J. F. Wu, M. Guo, Y. Yu, Z. L. Liu and J. K. Tang, *Inorg. Chem.*, 2019, **58**, 3167; (*c*) J. J. Lu, Y. Q. Zhang, X. L. Li, M. Guo, J. F. Wu, L. Zhao and J. K. Tang, *Inorg. Chem.*, 2019, **58**, 5715.

42 (*a*) Y. J. Gao, G. F. Xu, L. Zhao, J. K. Tang and Z. L. Liu, *Inorg. Chem.*, 2009, **48**, 11495; (*b*) L. Zhang, J. L. Jung, P. Zhang, M. Guo, L. Zhao, J. K. Tang and B. L. Guennic, *Chem. – Eur. J.*, 2016, **22**, 1392; (*c*) W. M. Wang, Z. L. Wu, Y. X. Zhang, H. Y. Wei, H. L. Gao and J. Z. Cui, *Inorg. Chem. Front.*, 2018, **5**, 2346; (*d*) C. Y. Xu, X. Y. Qiao, Y. Tan, S. S. Liu, W. Y. Hou, Y. Y. Cui, W. L. Wu, Y. P. Hua and W. M. Wang, *Polyhedron*, 2019, **160**, 272; (*e*) S. Y. Lin, L. Zhao, H. Ke, Y. N. Guo, J. K. Tang, Y. Guo and J. M. Dou, *Dalton Trans.*, 2012, **41**, 3248.

43 S. M. J. Aubin, Z. Sun, L. Pardi, J. Krzystek, K. Folting, L. C. Brunel, A. L. Rheingold, G. Christou and D. N. Hendrickson, *Inorg. Chem.*, 1999, **38**, 5329.